

Mesoscopic Concentration Fluctuations in a Fluidic Nanocavity Detected by Redox Cycling

Marcel A. G. Zevenbergen, Diego Krapf, Marc R. Zuiddam, and Serge G. Lemay*

Kavli Institute of Nanoscience, Section Molecular Biophysics, Delft University of Technology, Lorentzweg 1, 2628 CJ Delft, the Netherlands

Received November 2, 2006; Revised Manuscript Received November 29, 2006

ABSTRACT

We show that a nanofluidic device consisting of a solution-filled cavity bounded by two closely spaced parallel electrodes can amplify the electrical current from redox molecules inside the cavity by a factor of ~ 400 through redox cycling. The noise spectral density of this signal agrees quantitatively with the calculated fluctuations in the number of molecules inside the cavity due to their diffusive motion. We demonstrate sensitivity to fluctuations of as few as ~ 70 molecules.

The ability to locally detect few or individual molecules in solution is at present largely limited to fluorescence techniques, and a comparable method using electrical detection has so far remained elusive. Such a technique would be highly desirable for lab-on-a-chip applications and when labeling with fluorophores is invasive or impossible. More importantly, it would pave the way for fluidic devices in which individual ions are electrically detected and manipulated, allowing a new class of fundamental experiments on nonequilibrium statistical physics, transport at the molecular scale, and a broad range of biophysical systems.

Electrochemically active molecules are particularly amenable to electrical detection because they can transfer charge to appropriately biased electrodes. Electrochemical reactions involve one or a few electrons per reacting molecule, rendering the direct detection of a single molecule in solution virtually impossible. This obstacle can in principle be overcome through redox cycling, in which multiple electrodes are used to repeatedly flip the charge state of target molecules and thus allow each molecule to contribute multiple electrons to the measured current. Dual-band or interdigitated electrode microfluidic sensors have successfully employed this concept.¹ Recently, an amplification factor of 40 was reported for an interdigitated nanoelectrode array with 30 nm spacing,² and straightforward methods have been developed for fabricating dual-band electrode sensors with high collection efficiency.^{3–4} Redox cycling is also routinely used as feedback mechanism in scanning electrochemical microscopy.^{5–6} Single-molecule detection was claimed over a decade ago using the latter technique,⁵ but lack of control

and reproducibility has prevented the approach from evolving beyond the proof-of-concept stage.

Here we present a nanofluidic device that achieves highly sensitive electrical detection of electroactive ions through efficient redox cycling. The geometry of the device is carefully controlled and independently characterized, which allows a detailed comparison with theory. We analyze the noise spectral density of the measured electrical signal and demonstrate that it can be quantitatively explained by considering the diffusive motion of independent molecules in and out of the cavity. Fluctuations of as few as ~ 70 molecules can be detected in this manner.

The principle of operation of the device is schematically illustrated in Figure 1. Two closely spaced planar electrodes are biased such that the product of a reversible redox reaction at one electrode serves as reactant at the other, and vice-versa. Redox-active molecules diffusing in the cavity between the two electrodes sequentially shuttle multiple electrons, leading to a dramatic amplification of the electrochemical current.

The device fabrication process is sketched in Figure 2a–c. We started from Si wafers with 500 nm thermally grown wet SiO₂. A 30 nm thick Pt layer was evaporated onto this substrate and patterned using electron beam lithography and a lift-off process into a 12 $\mu\text{m} \times 12 \mu\text{m}$ bottom electrode with 3 μm wide wires leading to macroscopic contact pads. A 120 nm thick amorphous Si layer was then sputtered and patterned using lift-off into a 30 $\mu\text{m} \times 11 \mu\text{m}$ rectangle overlapping with the bottom electrode (Figure 2a). This sacrificial Si layer defined the shape and height of the fluidic cavity. Next, a 200 nm SiO₂ layer was sputtered over the whole device. A 10 $\mu\text{m} \times 10 \mu\text{m}$ well centered on the bottom

* Corresponding author. E-mail: s.g.lemay@tudelft.nl. Fax: +31-15-2781202.

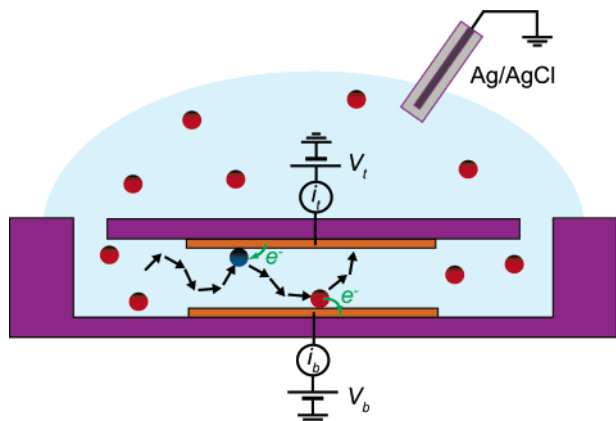


Figure 1. Illustration of the device concept. Redox-active molecules undergo a random walk between two closely spaced electrodes, shuttling electrons from one electrode to the other. V_t and V_b are the potentials applied to the top and bottom electrodes with respect to a Ag/AgCl reference electrode immersed in the bulk reservoir, while i_t and i_b are the corresponding measured currents.

electrode was etched through the oxide by CHF_3/O_2 reactive ion etching (RIE). A 60 nm thick top Pt electrode was then fabricated using the same techniques as the bottom electrode. It was positioned over the well in the SiO_2 layer to achieve a parallel plate geometry (Figure 2b). Next, a 350 nm SiO_2 capping layer was deposited into which two $3 \mu\text{m} \times 3 \mu\text{m}$ access holes were etched using RIE (Figure 2c). These holes served as access points for the plasma in the sacrificial etch process and, afterward, for filling the cavity with fluid. In a final step, the Si layer was sacrificially removed using a high-density inductively coupled SF_6 plasma. No oxygen was added, rendering the process isotropic.⁷ Atomic force microscopy (not shown) indicated that the top electrode buckled slightly upward, the final height of the cavity being ~ 300 nm. Parts e–f of Figure 2 show scanning electron micrographs of a finished device. The devices were cleaned using an oxygen plasma prior to experiments.

For measurements, ferrocenedimethanol ($\text{Fc}(\text{CH}_2\text{OH})_2$) (Aldrich) was chosen as electroactive species for its simple electrochemical behavior. Aqueous solutions were prepared from 18 M Ω cm Milli-Q water with 250 mM added KCl. A polydimethylsiloxane (PDMS) cell with two openings served as a 200 μL bulk reservoir. The $\sim 100 \mu\text{m}$ wide

bottom opening allowed the solution to contact the device, while a commercial 3 M Ag/AgCl reference electrode (BASi) was placed in the top opening to set the solution potential. The cavity was first wetted with ethanol, which was gradually replaced with aqueous solution. Current–voltage and current–time traces were recorded using a commercial bi-potentiostat (model CHI832B, CH Instruments).

Typical current–voltage measurements are shown in Figure 3. First, the potential applied to the bottom electrode was varied, while the top electrode was electrically floating. No redox cycling is possible under these conditions. The resulting current through the bottom electrode is shown as a dotted line and in the inset. This sigmoidal curve is characteristic of the reduced form of ferrocenedimethanol. The current saturates at a maximum of 27 pA, which is governed by mass transport from the bulk reservoir to the bottom electrode via the entrance holes.

Next, a constant potential of 0.10 V was applied to the top electrode, allowing redox cycling to take place. This change to the potential of the top electrode caused the electrochemical current through the bottom electrode to increase by a factor of ~ 400 (solid line, current saturates at 12.5 nA). The simultaneously measured current through the top electrode (dashed line) was the inverse of the current through the bottom electrode, confirming that nearly 100% of the generated product was cycled between the electrodes. Inverting the role of the two electrodes yielded equivalent results. Individual devices were stable for days, and results were reproducible using different devices.

Under the conditions used in our experiments, electron transfer between the molecules in solution and the electrodes is extremely fast and does not limit the measured current. In addition, because of the high concentration of inert salt, electric fields are strongly screened (Debye length < 1 nm) and transport of the redox species is due solely to diffusion. Neglecting fringing near the edges of the electrode, the transport-limited steady-state current $\langle i \rangle$ due to 1D diffusion between the two electrodes is

$$\langle i \rangle = \frac{eDL_A^2A_v c_0}{z} = \frac{e}{2\tau} \langle N \rangle \quad (1)$$

Here $-e$ is the electron charge, D the diffusion constant of

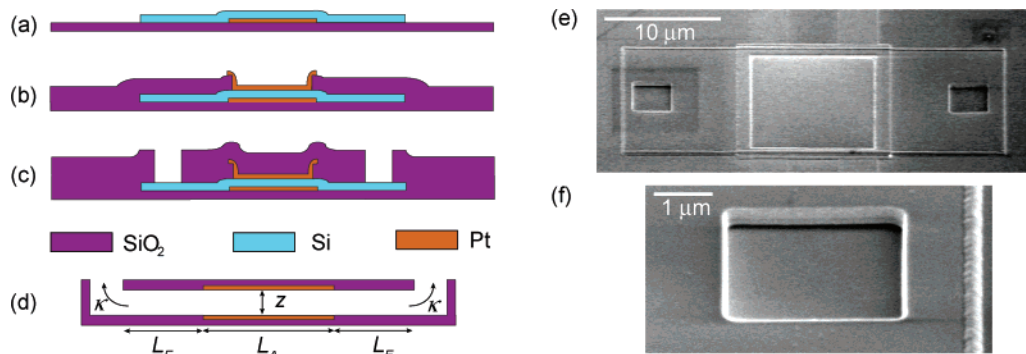


Figure 2. (a–c) Cross-section of the device at various stages of the fabrication process, as described in the text. (d) Simplified geometry used for theoretical modeling. (e) Scanning electron microscopy image of the final structure. (f) Magnification of the right entrance hole showing the fluidic cavity. (e) and (f) were taken at an angle of 40° .

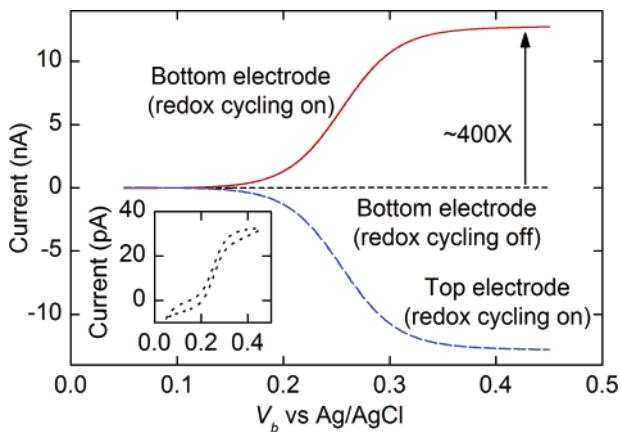


Figure 3. Current–voltage characteristics (cyclic voltammetry, scan rate 1 mV/s, $c_0 = 1$ mM) measured with the bottom electrode while the top electrode was disconnected (dotted line, magnification shown in inset) and while a potential of 0.10 V was applied to the top electrode (solid line). The dashed line represents the current through the top electrode obtained simultaneously with the solid line.

the redox ions (4.7×10^{-6} cm²/s),⁸ L_A^2 the area of overlap between the two electrodes ($100 \mu\text{m}^2$), A_V Avogadro’s number, c_0 the bulk redox-active ion concentration, z the distance between the electrodes, $\langle N \rangle = zL_A^2 A_V c_0$ the average number of particles in the active region of the device, and $\tau = z^2/2D$ the mean time to diffuse from one electrode to the other. A factor of 2 appears in the denominator of eq 1 because each ion crosses the gap twice per cycle.

Figure 4a shows the measured steady-state diffusion-limited current $\langle i \rangle$ versus electroactive ion concentration c_0 (squares). From a linear fit (solid red line) and eq 1, we determine the height of the cavity z to be 282 nm, consistent with the known cavity height.

Individual ions enter and leave the active region by diffusion, each ion residing in the active region for a time

of order $L_A^2/2D = 106$ ms. This is 3 orders of magnitude longer than the ion shuttling time $\tau = 85 \mu\text{s}$ deduced from the cavity height. On the time scale on which particles diffuse in and out of the active region, the shuttling dynamics are thus averaged out and each ion in the active region of the device contributes $e/2\tau = 0.95$ fA to the current. $i(t)$ thus provides a direct probe of the number of redox ions $N(t)$ in the cavity, and fluctuations in $i(t)$ reflect number fluctuations due to diffusive motion along the length of the channel.

To investigate these diffusion fluctuations, we recorded $i(t)$ for different concentrations under redox cycling conditions ($V_t = 0.50$ V, $V_b = 0.10$ V). Typical time traces for three concentrations are shown in Figure 4b (colored curves), together with a measurement of the background noise in the absence of redox cycling (gray curve, $V_t = V_b = 0.10$ V). It is readily apparent from these raw time traces that the noise amplitude increases with increasing number of ions in the cavity. Figure 4c shows the corresponding power spectral densities $S(f)$. All three spectra have the same shape, consisting of a low-frequency plateau and a power-law decay at high frequencies up to 10 Hz. Above 10 Hz, a faster decay is observed due to the finite bandwidth of the measurement electronics.

Diffusive fluctuations of the number of particles in a finite volume was treated by MacFarlane⁹ and by Van Vliet and Fasset,¹⁰ who predicted a white spectrum at low frequencies and a geometry-independent $f^{-3/2}$ “diffusion tail” at high frequencies. We fitted the data with the form

$$S(f) = \frac{S_0}{1 + \left(\frac{f}{f_0}\right)^{3/2}} \quad (2)$$

which interpolates between these limits. As shown by solid lines in Figure 4c, this empirical equation provides an excellent fit to the data.

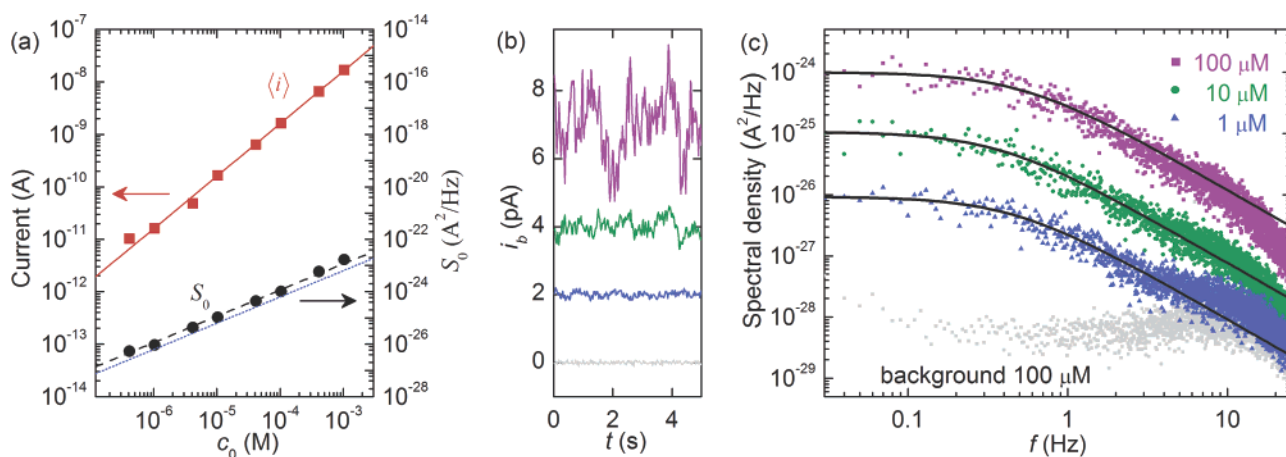


Figure 4. (a) Red squares show the measured diffusion-limited steady-state current $\langle i \rangle$ as a function of the redox molecule concentration. The solid red line is a fit to eq 1. The black circles show the measured low-frequency spectral density S_0 vs concentration. The dashed black line is a fit to $S_0 \propto c_0$, whereas the blue dotted line is calculated from the simplified geometry model of eq 3 without fitting parameters. The right-hand scale for S_0 is chosen such that the black circles also represent the rms current noise amplitude as per the left-hand scale.²¹ (b) Current time traces i_b for three concentrations of ferrocenedimethanol during redox cycling ($V_t = 0.50$ V, $V_b = 0.10$ V). The gray curve shows the background noise level with no redox cycling ($c_0 = 100 \mu\text{M}$, $V_t = V_b = 0.10$ V). The curves have been offset for clarity. (c) Spectral densities at the same concentrations. The solid lines are fits to eq 2.

The $f^{-3/2}$ diffusion tail has been rigorously observed for large (10 μm diameter) particles using light scattering.¹¹ It is not observed in corresponding molecular-scale correlation fluorescence spectroscopy experiments, however,¹² because in this case, the excitation domain consists of a Gaussian laser intensity distribution. The strength of the signal from each molecule then depends smoothly on its position in the domain, suppressing high-frequency fluctuations. $f^{-3/2}$ diffusion noise has been observed at the molecular scale in solid-state systems^{13–16} and in ionic transport experiments on electrolyte-filled capillaries,^{17–19} but in the latter case, contributions from volume flow had to be disentangled. It is unambiguously observed here because our device represents a near-ideal realization of the theoretical model, giving a signal that is directly proportional to the number of particles in a test volume with sharp boundaries.

To quantitatively compare our results to theory, we introduce a simplified 1D model of our device, as shown in Figure 1d. It consists of a central active region of length $L_A = 10 \mu\text{m}$ flanked by two access channels of length $L_E = 6 \mu\text{m}$. Neglecting particle exchange with the bulk reservoir, it is predicted that, in this simple geometry, the spectral density of the particle number exhibits a $f^{-3/2}$ diffusion tail at frequencies greater than $D/\pi(L_E + L_A/2)^2 = 1.2 \text{ Hz}$.¹⁰ This is in agreement with our data, as seen in Figure 4c.

At lower frequencies, exchange of molecules between the device volume and the reservoir adds a further contribution to the fluctuations. Bezrukov et al.²⁰ calculated the particle number fluctuations in a cylindrical nanopore opening onto large reservoirs. We extended their formalism to the geometry of Figure 2d. In this model, the time-dependent diffusion equation is solved explicitly inside the device, while the outward flux j_{out} from the device to the macroscopic reservoir via the entrance holes is described via a boundary condition. Namely, j_{out} is given by an escape rate constant κ times the local concentration at the ends of the access channels.

This calculation yields a simple analytical expression for S_0 , the spectral density at low frequencies:

$$S_0 = \langle N \rangle \left(\frac{e}{2\tau} \right)^2 \left(\frac{L_A^2}{3D} + 2 \frac{L_E L_A}{D} + 2 \frac{L_A}{\kappa} \right) \quad (3)$$

When $L_E \rightarrow 0$, the active part of the channel is directly connected to the reservoir and eq 3 reduces to the case of ref 20. When $L_E \neq 0$, the low-frequency noise is enhanced because particles exiting the active region have a high probability of returning after a short delay. Equation 3 indicates that $S_0 \propto \langle N \rangle \propto c_0$. This agrees with the experiment over 4 orders of magnitude as shown in Figure 4a and demonstrates that the fluctuations result from an incoherent superposition of contributions from independent molecules.

The value of the escape rate constant κ can be determined by equating the fluxes entering and leaving the channel at equilibrium.²⁰ Using finite element calculations (Comsol Multiphysics), we have determined the average steady-state flux of particles j_{in} reaching the channel entrance from bulk solution by diffusion. κ follows from $j_{\text{in}} = j_{\text{out}} = \kappa c_0$, yielding $\kappa = 2.3 \times 10^{-4} \text{ m/s}$.

All the constants in eq 3 are thus known; a direct comparison with our data is shown as the dotted blue line in Figure 4a. The idealized 1D model agrees with the spectral density data within a factor of ~ 2 without fitting parameter, indicating that it captures the essential functioning of the device. We attribute the slight discrepancy to simplifications of the geometry model, in particular the finite thickness of the bottom electrode, the 3D geometry of the access holes, and the different areas of the top and bottom electrodes exposed to solution.

For the smallest concentration investigated in Figure 4a, the rms amplitude of the fluctuations in the current is 67 fA.²¹ Since each molecule generates a current $e/2\tau = 0.95 \text{ fA}$, this indicates that we detect fluctuations of as few as ~ 70 molecules. Because $e/2\tau$ scales as z^{-2} , we expect that further downscaling of the device dimensions will make it possible to study individual molecules.

In summary, we have developed a nanofluidic device consisting of two planar electrodes separated by 300 nm. Redox cycling permits a ~ 400 -fold amplification of the electrochemical current. The concentration dependence of the fluctuations in this electrical signal, their high-frequency $f^{-3/2}$ behavior and their low-frequency amplitude demonstrate that the device acts as a direct probe of the diffusive motion of independent molecules.

Acknowledgment. We thank C. Dekker for useful discussions and general support. This work was funded by NanoNed and NWO.

References

- (1) For a comprehensive overview, see Amatore, C. in *Physical Electrochemistry*; Rubinstein I., Ed.; Marcel Dekker: New York, 1995; and references therein.
- (2) Ueno, K.; Hayashida, M.; Ye, J.; Misawa H. *Electrochem. Commun.* **2005**, *7*, 161–165.
- (3) Paixão, T. R. L. C.; Richter, E. M.; Brito-Neto, J. G. A.; Bertotti, M. *Electrochem. Commun.* **2006**, *8*, 9–14.
- (4) Ito, T.; Maruyama, K.; Sobue, K.; Ohya, S.; Niwa, O.; Suzuki, K. *Electroanalysis* **2004**, *16*, 2035–2041.
- (5) Fan, F. R. F.; Bard, A. J. *Science* **1995**, *267*, 871–874.
- (6) Mirkin, M. V. In *Scanning Electrochemical Microscopy*; Mirkin, M. V., Bard, A. J., Ed.; Marcel Dekker: New York, 2001.
- (7) Zuiddam, M. R.; Stein, D.; van der Heyden, F. H. J.; van der Drift, E. W. J. M.; Dekker, C. In preparation.
- (8) Determined from the diffusion-limited steady-state current of a Pt microelectrode (BASi, radius 5.5 μm determined optically) in 1 mM ferrocenedimethanol with 250 mM KCl as base electrolyte, in agreement with Zhang W.; Gaberman, I.; Ciszowska, M. *Electroanalysis* **2003**, *15*, 409–413.
- (9) MacFarlane, G. G. *Proc. Phys. Soc. B* **1950**, *63*, 807–814.
- (10) Van Vliet, K. M.; Fasset, J. R. In *Fluctuation Phenomena in Solids*; Burgess, R. E., Ed.; Academic Press: New York, 1965.
- (11) Voss, R. F.; Clarke J. J. *Phys. A: Math. Gen.* **1976**, *9*, 561–571.
- (12) Eigen, M.; Rigler, R. *Proc. Natl. Acad. Sci. U.S.A.* **1994**, *91*, 5740–5747.
- (13) Scofield, J. H.; Webb, W. W. *Phys. Rev. Lett.* **1985**, *54*, 353–356.
- (14) Rogers, C. T.; Myers, K. E.; Eckstein, J. N.; Bozovic, I. *Phys. Rev. Lett.* **1992**, *69*, 160–163.
- (15) Otten, F.; Kish, L. B.; Granqvist, C.-G.; Vandamme, L. K. J.; Vajtai R.; Kruijs, F. E.; Fissan, H. *Appl. Phys. Lett.* **2000**, *77*, 3421–3422.
- (16) Van der Ziel, A. *Noise in Solid-State Devices and Circuits*; John Wiley: New York, 1986.

- (17) Green, M. E. *J. Membr. Biol.* **1976**, 28, 181–186.
- (18) Van den Berg, R. J.; de Vos, A.; van der Boog, P.; de Goede, J. In *Proceedings of the 8th International Conference on Noise in Physical Systems and 1/f noise*; D'Amico, A., Mazzetti, P., Ed.; Elsevier: Amsterdam, 1986.
- (19) Weissman, M.; Feher, G. *J. Chem. Phys.* **1975**, 63, 586–587.
- (20) Bezrukov, S. M.; Berezhkovskii, A. M.; Pustuvoit M. A.; Szabo, A. *J. Chem. Phys.* **2000**, 113, 8206–8211.
- (21) For spectra described by eq 2, the rms current noise amplitude is $\delta i_{\text{rms}} = \sqrt{2S_0 f_0}$, where $f_0 = 0.42 \pm 0.03$ Hz in our experiments.

NL062571G